Journal of Computational Physics **168,** 356–383 (2001)
doi:10.1006/jcph.2001.6701, available online at http://www.idealibrary.com on IDEAL®

Solution of Cartesian and Curvilinear Quantum Equations via Multiwavelets on the Interval

Bruce R. Johnson, Jeffrey L. Mackey,[1] and James L. Kinsey

Department of Chemistry and Rice Quantum Institute, Rice University, MS 600, Houston, Texas 77251-1892
E-mail: johnson@rice.edu

Received July 26, 2000; revised December 11, 2000

It is shown how orthogonal compact-support multiwavelets may be used for the solution of quantum mechanical eigenvalue problems subject to specific boundary conditions. Special scaling functions and wavelets with convenient limiting behaviors at the edges of an interval are constructed in analogy to earlier work on single wavelet families. All of the integrals required for Hamiltonian matrix elements, involving both regular and edge functions, are calculated efficiently through use of recursion and quadrature methods. It is demonstrated through accurate eigenvalue determination that both Cartesian and curvilinear degrees of freedom are readily accommodated with such a basis, using as examples the particle in a box and the hydrogen atom in spherical polar coordinates.

Key Words: multiwavelets; interval; quantum; curvilinear; eigenvalue.

I. INTRODUCTION

The introduction of compact support wavelets by Daubechies [17, 18] raised the prospect of solving partial differential equations with functions resembling finite elements, but with automatic orthogonality and multiresolution properties. Previously, the development of general algorithms based on orthogonal functions providing highly customizable resolution would have seemed fantastic. At present, it merely seems difficult. A great deal of progress has occurred in the last several years. For example, many different varieties of such wavelet families [44] have now been derived, methods for calculation of integrals have been developed [4, 16, 34, 38, 51], and there are efficient means for dealing with operators expressed in multiscale bases [5]. Early applications naturally gravitated toward differential equations with strongly specific local behavior, e.g., differential equations modeling shock wave fronts in fluids [25, 39, 41, 43, 56], which may be solved by Wavelet-Galerkin [25, 39, 41, 53, 55, 71] or Wavelet Collocation [3, 61, 62] methods.

[1] Permanent address: Micron Technology, Inc., MS 306, 8000 Federal Way, Boise, Idaho 83707-0006.

0021-9991/01 $35.00

Our specific interest is in the application to quantum mechanical problems involving atoms and molecules, for which much the same numerical machinery is needed. A number of quantum mechanical wavelet investigations have already been undertaken [1, 6, 9, 20–23, 26–29, 31, 34, 49, 60, 65, 66], though some of these studies have preferred nonorthogonal wavelets for reasons concerning sampling properties, smoothness, and so forth. Presently, somewhat ironically, one is probably more limited in the ability to use the orthogonal compact-support wavelets, even though these are the functions that fueled the initial widespread interest in wavelet applications. For example, it was not until 1996 (to our knowledge) that it was even demonstrated that Daubechies wavelets could be used systematically in accurate eigenvalue determination for Hamiltonians with general classes of potentials [49]. There are still residual issues however. The combination of orthogonality and compact support properties disallows symmetry of the basis functions [18], leading unavoidably to either a left or right bias on the support. Moreover, wavelets are generally defined along infinitely long Cartesian axes. This ignores the large number of physical problems most naturally expressed in curvilinear coordinates, as well as Cartesian problems possessing hard potential walls.

The issue of left–right democracy may be handled by adopting one of the wavelet variations that accommodates both compact support and symmetry properties. One of these, biorthogonal wavelets, would unfortunately require giving up the hermiticity of the Hamiltonian matrix. Another variation, multiwavelets, offers symmetry, greater localization, and hermiticity at the price of increasing the number of distinct functional shapes to be included in the basis. Currently, the primary handicap to the use of multiwavelets is probably lack of examples of their use, one of the problems addressed in this paper. The specific choice made here is the multiwavelet family of Chui and Lian [10], symmetric and antisymmetric pairs of functions defined on the interval [0,3]. All of the necessary tools for calculation of the kinetic and potential energy matrix elements with this basis are given below, providing a multiwavelet generalization of results for the single (or scalar) wavelet families [4, 16, 34, 38, 54].

The issue of curvilinear coordinates is important throughout a huge variety of electronic and nuclear applications. One finds use made of spherical, parabolic, elliptical, and other coordinates [52] in atomic physics, as well as radial and angular variables from valence bond, Jacobi, hyperspherical [58], Radau [35], and several other types of coordinates arising in molecular physics. In special cases, curvilinear coordinates are used because they allow a separation of variables, but they are also frequently used because they simplify nonseparable multidimensional problems (e.g., for reasons of symmetry). The lack of compact support wavelets constructed specifically for use with curvilinear coordinates has appeared to be a general limitation of wavelet techniques. In many cases, however, the differences offered by curvilinear coordinates can be reduced to (i) a restriction of the domain of definition to either a half-line or a finite interval and (ii) simple algebraic singularities at the domain edge(s). The first point also occurs in Cartesian problems, such as the particle in a box, for which the potential restricts motion to a finite interval. For single wavelet systems [2, 12, 13, 46, 50, 51] and, more recently, for biorthogonal multiwavelets [14], special functions have been constructed that complement the regular basis functions in order to adapt the multiresolution analysis adapted to a fixed interval. This approach is complementary to the recent body of work on the use of Wavelet-Galerkin methods for partial differential equations in bounded domains [7, 8, 11, 15, 19, 24, 36, 37, 63, 67].

In this paper, a method similar to that of Monasse and Perrier [51] is used to construct edge functions for the Chui–Lian multiwavelet basis. These "multiwavelets on the interval" are suited to the satisfaction of one- and two-point boundary conditions for the example quantum systems—the particle in a box and the angular and radial equations arising from the separation of variables for the hydrogen atom—and many others. It has not been possible previously to obtain eigenvalues for such problems with more than a few digits of accuracy, even using single orthogonal wavelet families, much less multiwavelets. The basis will also provide tailored resolution in solutions of the time-dependent Schrödinger equation in curvilinear coordinates. The price we must pay for all this is the evaluation of a significant number of key integrals involving differential and local operators and involving Chui–Lian functions and their edge counterparts, even though symmetry properties are used as much as possible to reduce the number of independent integrals required. While these first demonstrations are specific to the Chui–Lian multiwavelet family, it is expected that such evaluations for other wavelet or multiwavelet families can be largely automated.

II. MULTIWAVELETS ON THE FULL LINE

The two scaling functions $\{\phi_1(x), \phi_2(x)\}$ and the two wavelets $\{\psi_1(x), \psi_2(x)\}$ defined by Chui and Lian are shown in Fig. 1. All of these functions have unit L^2 norm. Letting

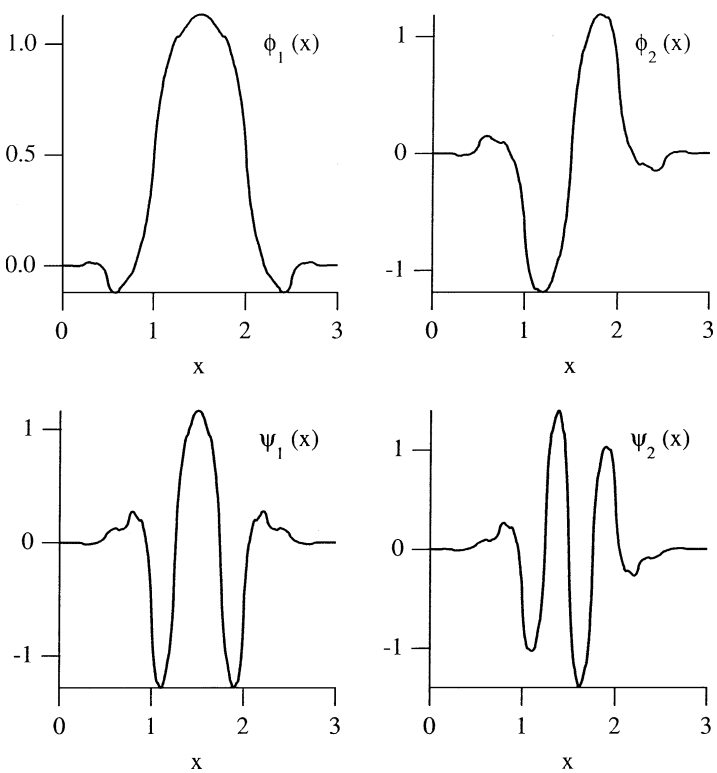

FIG. 1. Scaling functions and wavelets of the Chui–Lian multiwavelet family on the interval [0,3].

$\hat{\phi} = (\phi_1, \phi_2)^T$ and $\hat{\psi} = (\psi_1, \psi_2)^T$, these vectors obey the two-scale relations

$$\hat{\phi}(x) = \sum_{k=0}^{3} \mathbf{c}_k \hat{\phi}(2x - k), \tag{1}$$

$$\hat{\psi}(x) = \sum_{k=0}^{3} \mathbf{d}_k \hat{\phi}(2x - k), \tag{2}$$

representing a matrix version of the relations obeyed by the Daubechies wavelet families. The coefficients $\mathbf{c}_k$ and $\mathbf{d}_k$ are 2×2 constant matrices given in the Appendix. Square-normalized copies of these functions that are squeezed by $1/2^j$ and shifted by $k/2^j$ for integral j and k are given by

$$\phi_{jk\alpha}(x) = 2^{j/2} \phi_\alpha(2^j x - k), \tag{3}$$

$$\psi_{jk\alpha}(x) = 2^{j/2} \psi_\alpha(2^j x - k). \tag{4}$$

A complete orthonormal basis can be specified by choosing a coarsest scale, which we shall denote for convenience as $j = 0$, and including all $j = 0$ scaling functions and all $j \geq 0$ wavelets. Thus, a function $f(x)$ expanded in this set takes the form

$$f(x) = \sum_{k=-\infty}^{+\infty} \sum_{\alpha=1}^{2} \langle \phi_{0k\alpha} \mid f \rangle \phi_{0k\alpha}(x) + \sum_{j=0}^{+\infty} \sum_{k=-\infty}^{+\infty} \sum_{\alpha=1}^{2} \langle \psi_{jk\alpha} \mid f \rangle \psi_{jk\alpha}(x). \tag{5}$$

(In the following we shall use the conventions that two subscripts implies $j = 0$, i.e., $\phi_{k\alpha} \equiv \phi_{0k\alpha}$ and $\psi_{k\alpha} \equiv \psi_{0k\alpha}$, while one subscript implies $j = 0$ and $k = 0$, i.e., $\phi_\alpha \equiv \phi_{00\alpha}$ and $\psi_\alpha \equiv \psi_{00\alpha}$.) Finite basis calculations are then implemented by retaining only some maximum number J of scales ($0 \leq j < J$) and restricting each sum over k to include only those values in a region or regions of interest,

$$f(x) \approx \sum_{k} \sum_{\alpha=1}^{2} \langle \phi_{k\alpha} \mid f \rangle \, \phi_{k\alpha}(x) + \sum_{j=0}^{J-1} \sum_{k} \sum_{\alpha=1}^{2} \langle \psi_{jk\alpha} \mid f \rangle \, \psi_{jk\alpha}(x). \tag{6}$$

A constraint that enters into the constuction of the multiwavelet system is that Eq. (1) represents coarsening (lowpass filtering), and Eq. (2) represents selection of details (highpass filtering). This is partially ensured by requiring that the multiwavelets ψ_α are orthogonal to low-order polynomials. As a consequence, these polynomials are precisely contained within the space of the scaling functions. We have the exact equality

$$P(x) = \sum_{k} \sum_{\alpha=1}^{2} \langle \phi_{k\alpha} \mid P \rangle \, \phi_{k\alpha}(x), \tag{7}$$

provided that $P(x)$ is at most a quadratic polynomial. The Chui–Lian multiwavelet family is said to be of *approximation order* three since the three powers x^0, x^1, and x^2 can be exactly expressed as linear combinations of the multiscaling functions [10]. Evaluation of the projections of powers onto the multiscaling functions can be accomplished by use of

Eq. (1), as shown in a separate paper [32]. We define the moments

$$m_{p\alpha}(\kappa) = \int dx\, x^p \phi_\alpha(x-\kappa) = \int dx (x+\kappa)^p \phi_\alpha(x), \tag{8}$$

where the shift κ is not necessarily integral. Then Eq. (1) implies that the vector equation

$$\hat{\mathrm{m}}_p(\kappa) = \begin{pmatrix} m_{p1} \\ m_{p2} \end{pmatrix}(\kappa) = \frac{1}{2^p} \sum_{p'=0}^{p} \binom{p}{p'} \boldsymbol{\mu}_{p-p'}(\kappa) \hat{\mathrm{m}}_{p'}(\kappa) \tag{9}$$

must be satisfied, where the matrix

$$\boldsymbol{\mu}_p(\kappa) = \frac{1}{2} \sum_{k=0}^{3} \mathbf{c}_k (\kappa + k)^p \tag{10}$$

is easily calculated. In the particular case $p = 0$, Eq. (9) reduces to

$$\hat{\mathrm{m}}_0 = \boldsymbol{\mu}_0 \cdot \hat{\mathrm{m}}_0, \tag{11}$$

i.e., $\hat{\mathrm{m}}_0$ is an eigenvector of $\boldsymbol{\mu}_0$ with eigenvalue 1. For the current multiwavelets, the initial moments are given by $\hat{\mathrm{m}}_0 = [1, 0]^T$, independent of κ. All higher projections follow from Eq. (9). By choosing $\kappa = -3/2$, symmetry gives the simplifications that odd moments vanish for $\alpha = 1$ and even moments vanish for $\alpha = 2$. The first few nonzero moments are given in Table I. For more general κ, the moments may be calculated in terms of these:

$$\begin{aligned} m_{p\alpha}(\kappa) &= \int dx \left(x - \frac{3}{2} + \kappa + \frac{3}{2} \right)^p \phi_\alpha(x) \\ &= \sum_{p'=0}^{p} \binom{p}{p'} \left(\kappa + \frac{3}{2} \right)^{p-p'} \int dx \left(x - \frac{3}{2} \right)^{p'} \phi_\alpha(y) \\ &= \sum_{p'=0}^{p} \binom{p}{p'} \left(\kappa + \frac{3}{2} \right)^{p-p'} m_{p'\alpha}\left(-\frac{3}{2} \right). \end{aligned} \tag{12}$$

TABLE I

Lowest-Order Nonzero Moments of the Chui–Lian Scaling Functions for $\kappa = -3/2$

p	$m_{2p,1}(-3/2)$	$m_{2p+1,2}(-3/2)$
0	1	$\frac{\sqrt{15}-\sqrt{6}}{6}$
1	$\frac{7-2\sqrt{10}}{12}$	$\frac{319\sqrt{15}-505\sqrt{6}}{1992}$
2	$\frac{1011-324\sqrt{10}}{1328}$	$\frac{24937441\sqrt{15}-40418461\sqrt{6}}{105392736}$
3	$\frac{199096521-63748426\sqrt{10}}{163944256}$	$\frac{1349132289413\sqrt{15}-2159493518895\sqrt{6}}{3384231014784}$

III. MULTISCALING FUNCTIONS ON THE INTERVAL

For situations where it is desired to use a basis restricted to a finite or semi-infinite interval, most orthogonal wavelet families are deficient. The problem comes from the staggered supports of the scaling functions and wavelets. There will always be some basis functions which straddle any boundary. Retaining such basis functions is not appropriate since they have tails outside the region of interest (with longer tails for coarser scales). On the other hand, neglecting them is also inappropriate since the tails inside the region are critical for the basis to reproduce low-order polynomials near the edges. A common workaround for a finite interval is to use periodized scaling functions and wavelets which wrap around the domain edges [59]. However, this has the undesirable effect of artificially destroying some of the very localization which was such an appealing aspect of wavelet bases.

An alternative pursued by Meyer [46] was to include just the inner tails as independent basis functions, but these were not generally orthogonal to each other and were subject to problems of numerical precision. Subsequent work by Cohen *et al.* [12, 13], showed how to use the restrictions of the primitive edge scaling functions and wavelets in linear combination to obtain special edge functions orthogonal both to each other and to all the basis functions away from the edge. Monasse and Perrier [50, 51], extending results of Auscher [2], showed a similar construction which gave special edge functions adapted naturally to the solution of particular (e.g., Dirichlet or Neuman) differential equation boundary conditions. The latter approach is further extended in the present paper to orthogonal multiwavelets, working with the specific case of the Chui–Lian family and specializing to boundary conditions commonly met in the standard problems of quantum mechanics.

We start by considering a left-hand boundary situated at $x = 0$. The functions $\phi_{k\alpha}$ and $\psi_{k\alpha}$ for $k \geq 0$ are entirely to the right, while those for $k = -1$ and -2 straddle the origin. The monomial expansions take the forms

$$x^p = \sum_{\alpha=1}^{2} \sum_{k} m_{p\alpha}(k)\phi_{k\alpha}(x), \quad p = 0, 1, 2. \tag{13}$$

If the sum over k in Eq. (13) starts at $k = 0$, then the equality holds for all $x \geq 2$. To obtain equality for all $x \geq 0$, we only need to add the right-hand tails of the $k = -1$ and -2 functions. In terms of the Heaviside function $\Theta(x) = 1$ for $x > 0$, 0 for $x < 0$,

$$\Theta(x)x^p = \sum_{k=-2}^{\infty} \sum_{\alpha=1}^{2} m_{p\alpha}(k)\Theta(x)\phi_{k\alpha}(x). \tag{14}$$

At least three edge scaling functions are needed to restore approximation order three for all $x \geq 0$. We choose these to be of the same length as the other scaling functions, having support [0, 3]. In analogy to the scalar wavelet procedure adopted by Cohen *et al.* [13], the $k = 0$ functions (for which [0, 3] is the support) are borrowed for this purpose instead of being included in the set of regular scaling functions. Thus, in terms of the three independent left-hand edge functions,

$$\phi_p^L(x) = \sum_{k=-2}^{0} \sum_{\alpha=1}^{2} m_{p\alpha}(k)\Theta(x)\phi_{k\alpha}(x), \tag{15}$$

Eq. (14) can be rewritten as

$$\Theta(x)x^p = \phi_p^L(x) + \sum_{k=1}^{\infty}\sum_{\alpha=1}^{2} m_{p\alpha}(k)\phi_{k\alpha}(x). \tag{16}$$

These functions are orthogonal to all of the $\phi_{k\alpha}$ for $k \geq 1$ by construction, but they are not orthogonal to each other. It is first necessary to find the overlap matrix with integrations restricted to $x \geq 0$,

$$\lambda_{\ell,\beta;k,\alpha} = \int dx\, \Theta(x)\phi_{\ell;\beta}(x)\phi_{k;\alpha}(x). \tag{17}$$

Using the recursion relation in Eq. (1) for both scaling functions leads to the identity

$$\lambda_{\ell,\beta;k,\alpha} = \frac{1}{2}\sum_{\ell'=0}^{3}\sum_{\beta'=1}^{2}\sum_{k'=0}^{3}\sum_{\alpha'=1}^{2} c_{\ell',\beta,\beta'}c_{k',\alpha,\alpha'}\lambda_{2\ell+\ell',\beta';2k+k',\alpha'}. \tag{18}$$

All integrals for which either of the first or third subscripts is ≥ 0 reduce to the standard orthogonality integrals. Equations (18) then become a series of inhomogeneous equations for those with both subscripts <0. Solving for these truncated integrals yields the values appearing in Table II. According to Eq. (15), the overlaps among the $\phi_p^L(x)$ are then given by

$$\begin{aligned} S_{p'p} &= \int dx\, \phi_{p'}^L(x)\phi_p^L(x) \\ &= \sum_{\ell=-2}^{0}\sum_{\beta=1}^{2}\sum_{k=-2}^{0}\sum_{\alpha=1}^{2} m_{q\beta}(\ell)m_{p\alpha}(k)\lambda_{\ell\beta;k\alpha}. \end{aligned} \tag{19}$$

TABLE II

Upper Triangle Overlap Matrix Elements $\lambda_{\ell,\beta;k,\alpha}$ for $k, \ell < 0$

ℓ	β	k	α	$\lambda_{\ell,\beta;k,\alpha}$
−2	1	−2	1	$\frac{10 - 3\sqrt{10}}{40}$
−2	1	−2	2	$\frac{47\sqrt{15} - 70\sqrt{6}}{750}$
−2	1	−1	1	0
−2	1	−1	2	$\frac{-35\sqrt{6} - 14\sqrt{15}}{9000}$
−2	2	−2	2	$\frac{710 - 209\sqrt{10}}{3000}$
−2	2	−1	1	$\frac{-35\sqrt{6} - 14\sqrt{15}}{9000}$
−2	2	−1	2	0
−1	1	−1	1	$\frac{3 + 3\sqrt{10}}{40}$
−1	1	−1	2	$\frac{47\sqrt{15} - 70\sqrt{6}}{750}$
−1	2	−1	2	$\frac{2290 + 209\sqrt{10}}{3000}$

This matrix takes the simple form

$$\mathbf{S}^L = \begin{pmatrix} 2 & \frac{27-\sqrt{10}}{12} & \frac{11-\sqrt{10}}{3} \\ \frac{27-\sqrt{10}}{12} & \frac{11-\sqrt{10}}{3} & \frac{1276-185\sqrt{10}}{180} \\ \frac{11-\sqrt{10}}{3} & \frac{1276-185\sqrt{10}}{180} & \frac{136-26\sqrt{10}}{9} \end{pmatrix}. \tag{20}$$

The final step in constructing edge scaling functions is to make them orthogonal to each other. Monasse and Perrier discuss the possibility of different choices based on different types of boundary conditions (e.g., Dirichlet or Neuman). Our particular interest is to use these functions for second-order differential equations of quantum mechanics, in which case it is frequently convenient to be able to specify the wave function's lowest-order (indicial) power of x as $x \to 0$. It is therefore natural for our purposes to start Gramm–Schmitt orthogonalization with the x^2 function, orthogonalize the x^1 function with respect to it, and then to orthogonalize the x^0 solution to the previous two. Defining the orthogonalized functions to be $\Phi_n^L(x)$, $n = 0, 1, 2$, we have

$$\hat{\Phi}^L = \mathbf{T}\hat{\phi}^L, \tag{21}$$

where

$$\mathbf{T} = \begin{pmatrix} 2.183415683967980 & -4.591492847717150 & 1.994990649446751 \\ 0 & 2.612321037529930 & -1.678162710805578 \\ 0 & 0 & 0.4090794873451215 \end{pmatrix}, \tag{22}$$

and where $\mathbf{T}$ is upper-diagonal. The resulting orthogonal edge functions are shown in Fig. 2.

The recursion satisfied by the edge scaling functions is necessarily mixed with the regular scaling functions. This can be seen by tracking back through the cumulative transformations to the definitions of the scaling function tails, for which Eq. (1) applies. We use the notation $\chi_{[0,3]}(x)$ for the unit pulse between 0 and 3, i.e., $\Theta(x)\Theta(3-x)$. Using Eqs. (1), (16), and

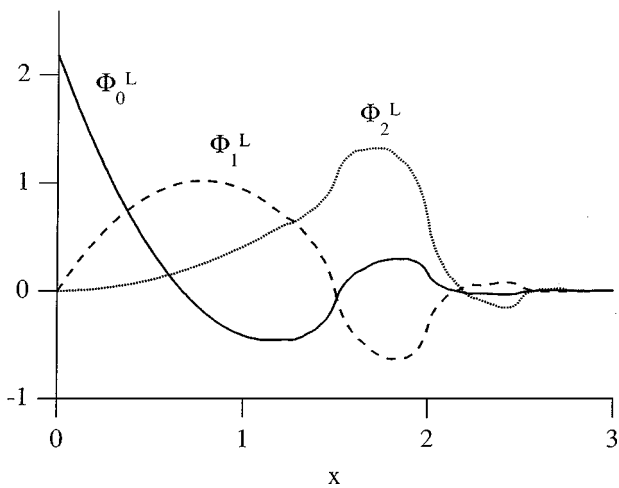

FIG. 2. Orthogonal left-hand edge scaling functions $\Phi_n^L(x)$ behaving as x^n near $x = 0$.

the inverse of Eq. (21), $\hat{\phi}^L = \mathbf{T}^{-1}\hat{\Phi}^L$, we find

$$\begin{aligned}\Phi_n^L(x) &= \sum_p T_{np}\phi_p^L(x) = \chi_{[0,3]}(x)\sum_p T_{np}\left[x^p - \sum_{k=1}^{2}\sum_{\alpha=1}^{2} m_{p\alpha}(k)\phi_\alpha(x-k)\right] \\ &= \chi_{[0,3]}(x)\left[\sum_p T_{np}\,\frac{1}{2^p}\,\phi_p^L(2x) + \sum_p T_{np}\frac{1}{2^p}\sum_{k=1}^{\infty}\sum_{\alpha=1}^{2} m_{p\alpha}(k)\phi_\alpha(2x-k)\right. \\ &\quad \left. - \sum_p T_{np}\sum_{k=1}^{2}\sum_{\alpha=1}^{2} m_{p\alpha}(k)\sum_{k'=0}^{3}\sum_{\alpha'=1}^{2} c_{k\alpha;k'\alpha'}\phi_{\alpha'}(2x-2k-k')\right] \\ &= \sum_{p=0}^{2} A_{np}\Phi_p^L(2x) + \sum_{k=1}^{3}\sum_{\alpha=1}^{2} B_{n;k\alpha}\phi_\alpha(2x-k), \end{aligned} \tag{23}$$

where

$$\mathbf{A} = \begin{pmatrix} 1 & 0.8788148129103263 & -0.05243171319728923 \\ 0 & 0.5 & 1.025572512628694 \\ 0 & 0 & 0.25 \end{pmatrix}, \tag{24}$$

$$\mathbf{B} = \begin{pmatrix} -0.4107044479981856 & 0.04697336433775339 & 0.2238144195138839 \\ 0.6196573513907207 & -0.1877927019856355 & -0.5178992870836935 \\ 0.6449431690452238 & 0.1213170903183015 & 1.217841280627102 \\ 0.05713560994297492 & -0.006513435024601166 & -0.02551474781712300 \\ -0.08462384368043302 & 0.009647081879315406 & 0.05904029656940184 \\ -0.06604312939516946 & 0.007528888421180750 & -0.1388333835861504 \end{pmatrix}. \tag{25}$$

These matrices satisfy the normalization condition,

$$\mathbf{A}\cdot\mathbf{A}^T + \mathbf{B}\cdot\mathbf{B}^T = 2\mathbf{I}_3, \tag{26}$$

where $\mathbf{I}_3$ is the 3×3 identity matrix.

The moments

$$M_{pn}^L = \int dx\, x^p\, \Phi_n^L(x) \tag{27}$$

can be calculated using Eq. (23),

$$\begin{aligned} M_{pn}^L &= \sum_{n'=0}^{2} A_{nn'}\int dx\, x^p\, \Phi_{n'}^L(2x) + \sum_{k=1}^{3}\sum_{\alpha=1}^{2} B_{n;k\alpha}\int dx\, x^p\phi_\alpha(2x-k) \\ &= 2^{-p-1}\sum_{n'=0}^{2} A_{nn'}M_{pn'}^L + 2^{-p-1}\sum_{k=1}^{3}\sum_{\alpha=1}^{2} B_{n;k\alpha}m_{p\alpha}(k)\cdot \end{aligned} \tag{28}$$

TABLE III
Lowest Order Edge Scaling Function Moments

p	M^L_{p0}	M^L_{p1}	M^L_{p2}
0	0.4579979924769402	0.8049908401438545	1.068750478910575
1	0	0.3828013424205878	1.570362138335678
2	0	0	2.444512694806293
3	0.1465181581638399	−0.5399850568182881	3.932629848953578
4	0.4552905009099832	−1.423442829785282	6.443219022311416
5	1.011352504926067	−2.903380061865061	10.63546210201256
6	1.938732345356721	−5.320657502573146	17.51075456849672

So,

$$M^L_{pn} = \sum_{n'=0}^{2} (2^{p+1}\mathbf{I} - \mathbf{A})^{-1}_{nn'} \sum_{k=1}^{3} \sum_{\alpha=1}^{2} B_{n';k\alpha} m_{p\alpha}(k). \tag{29}$$

The moments for the first few values of p are tabulated in Table III.

IV. MULTIWAVELETS ON THE INTERVAL

Following Cohen *et al.* [13], a primitive set of edge wavelets may be constructed by considering what is left over from $\Phi^L_n(2x)$ after subtraction of the projection onto the $\Phi^L_{n'}(x)$,

$$\begin{aligned}\tilde{\Psi}^L_n(x) &= \Phi^L_n(2x) - \sum_{n'=0}^{2} \Phi^L_{n'}(x) \int dx'\, \Phi^L_n(2x')\, \Phi^L_{n'}(x') \\ &= \Phi^L_n(2x) - \frac{1}{2} \sum_{n'=0}^{2} A_{n'n} \Phi^L_{n'}(x). \end{aligned} \tag{30}$$

These functions are, by construction, orthogonal to all of the edge scaling functions $\Phi^L_{n'}(x)$. They are also orthogonal to all of the inner scaling functions $\phi_{k,\alpha}(x)$ and wavelets $\psi_{k,\alpha}(x)$ for $k \geq 1$. This is obviously true for the $\Phi^L_{n'}(x)$ terms since they are on the same scale. This can also be seen for the first term on the right-hand side by expressing the $\phi_{k,\alpha}(x)$ and $\psi_{k,\alpha}(x)$ for $k \geq 1$ in terms of the $\phi_{k,\alpha}(2x)$ for $k \geq 2$, all of which are orthogonal to $\Phi^L_n(2x)$.

The orthogonal set of edge wavelets is constructed from linear combinations of these functions,

$$\Psi^L_n(x) = \sum_{n'=0}^{2} U_{nn'} \tilde{\Psi}^L_{n'}(x). \tag{31}$$

These obey refinement relations analogous to Eq. (23),

$$\Psi^L_n(x) = \sum_{n'=0}^{2} F_{nn'}\, \Phi^L_{n'}(2x) + \sum_{k=1}^{3} \sum_{\alpha=1}^{2} G_{n;k\alpha}\, \phi_\alpha(2x-k), \tag{32}$$

for which normalization and orthogonality to edge scaling functions requires

$$\mathbf{F}\cdot\mathbf{F}^T+\mathbf{G}\cdot\mathbf{G}^T=2\mathbf{I}_3, \tag{33}$$

$$\mathbf{F}\cdot\mathbf{A}^T+\mathbf{G}\cdot\mathbf{B}^T=0. \tag{34}$$

Furthermore, we ask that $\Psi_n^L(x)\sim x^n$ as $x\to 0$ in the same manner as was done for the $\Phi_n^L(x)$. The solutions to these equations are

$$\mathbf{U}=\begin{pmatrix} 2 & 0 & 0\\ 3.878464922835441 & 4.413290338144536 & 0\\ 25.57235065307173 & 29.97173655985489 & 14.63342236191503\end{pmatrix}, \tag{35}$$

$$\mathbf{F}=\begin{pmatrix} 1 & -0.8788148129103263 & 0.05243171319728923\\ 0 & 0.453176620335777 & -0.9281827547828538\\ 0 & 0 & 0.1366734281657313\end{pmatrix}, \tag{36}$$

$$\mathbf{G}=\begin{pmatrix} 0.4107044479981856 & -0.04697336433775339 & -0.2238144195138839\\ 0.9092208447502303 & 0.02501138342026960 & -0.2966463953547730\\ 0.03011480499895239 & 1.393150708972995 & -0.1843018711234421\\ -0.05713560994297492 & 0.006513435024601166 & 0.02551474781712300\\ -0.1282310610857589 & 0.01461828595776544 & 0.03381756182097140\\ -0.07120442861293362 & 0.008117274318014343 & 0.02101033424992004\end{pmatrix}. \tag{37}$$

The corresponding edge wavelets are shown in Fig. 3.

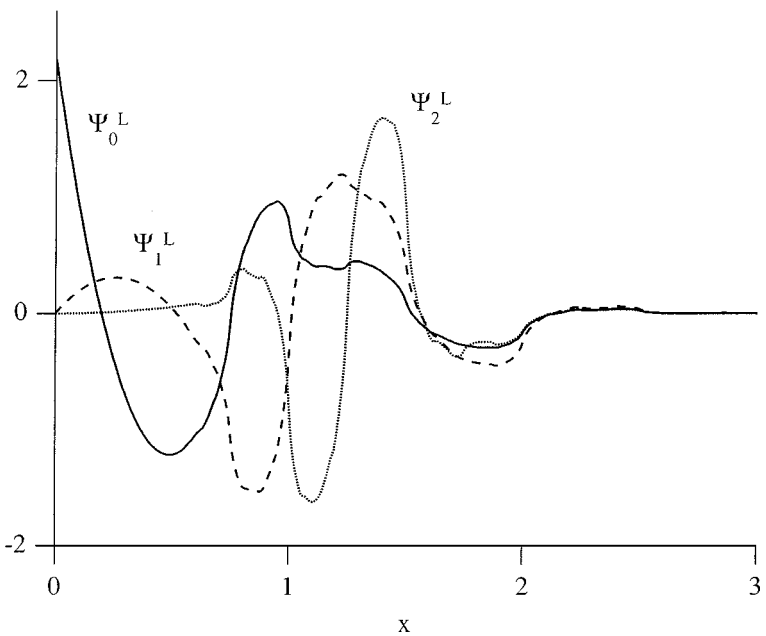

FIG. 3. Orthogonal left-hand edge wavelets $\Psi_n^L(x)$ behaving as x^n near $x=0$.

Because of the symmetry of the underlying basis, a right-hand boundary can be simply accommodated by using the mirror images of the $\Phi_p^L(x)$ and $\Psi_p^L(x)$ [13]. Thus, all functions necessary for maintaining approximation order 3 in the presence of left-hand edges, right-hand edges, or both have been obtained. The one caveat is that it is assumed that, for finite intervals, there are sufficient inner functions that the left-hand and right-hand edge functions do not overlap.

V. LINEAR MOMENTS AND GENERAL PROJECTION INTEGRALS

For expansion of general functions, $f(x)$, it is necessary to resort to approximate methods for the evaluation of the projection integrals. If projections on a fine scale J are accurately calculated, the scaling function and wavelet projections on coarser scales may be obtained using the two-scale recursions. In the frequently used Mallat algorithm [45] for single wavelet systems, the level-J integrations are approximated by samples $f(k/2^J)$ under the assumption that $f(x)$ is slowly varying relative to this scale. This has the strong convenience that the lowpass and highpass recursions can be iterated starting directly from the data sequence. Sufficient accuracy is not always obtained for the wavelet and scaling function coefficients on the various scales however [33, 34], and there is not a natural generalization to the case of multiwavelet families, which need multiple input data streams. Both of these issues may be addressed by prefiltering of the input sequence of samples [30, 47, 59, 64, 68–70], to borrow from the language of signal processing.

A projection-based prefiltering using polynomial interpolation has been shown to markedly improve accuracy for nonsingular functions $f(x)$ in either single wavelet [33, 34] or multiwavelet [32] families using a few samples that fall within the neighborhood of each of the level-J scaling functions. For a particular value of k, one approximates $f(x)$ in terms of its samples at positions x_{Jkq}, $q = 1, 2, \ldots, r$,

$$f(x) \approx \sum_{q=1}^{r} L_{Jkq}(x)\, f(x_{Jkq}). \tag{38}$$

In the most common circumstance, the positions are equally spaced and have the form

$$x_{Jkq} = \frac{k + \delta + q - 1}{2^J}, \tag{39}$$

where δ is a constant shift which may be chosen as convenient in aligning the sample positions with respect to the support $[k/2^J, (k+3)/2^J]$ of $\phi_{Jk\alpha}$. However, it is not necessary in the following derivations for the points to be distributed regularly. In any case, the $L_{Jkq}(x)$ are Lagrange interpolating polynomials of order $r-1$,

$$L_{Jkq}(x) = \prod_{q' \neq q}^{r} \frac{x - x_{Jkq'}}{x_{Jkq} - x_{Jkq'}}, \tag{40}$$

taking the value 1 at $x = x_{Jkq}$ and 0 at the other sample points. Equation (38) is an equality for $f(x)$ in the form of a polynomial of order up to $r-1$ and an approximate equality otherwise.

From this form, we obtain a numerical quadrature approximation for the projection integrals,

$$\langle \phi_{Jk\alpha} \mid f \rangle \approx \sum_{q=1}^{r} \omega_{Jk\alpha q} f(x_{Jkq}). \tag{41}$$

Here the $\omega_{Jk\alpha q}$ are the quadrature weights, which may be expressed in terms of the moments in Eq. (8) and derivatives of the Lagrange polynomials,

$$\omega_{Jk\alpha q} = \sum_{p=0}^{r-1} 2^{-J/2-Jp} \frac{m_{p\alpha}(-\delta)}{p!} L^{(p)}_{Jkq}\left(\frac{k+\delta}{2^J}\right). \tag{42}$$

Each of the terms in Eq. (42) is factored into a moment which depends on scaling function characteristics and an algebraic part which depends on the grid (x_{Jkq}). The moments need to be evaluated only once.

Frequently it will be the case that the sets of x_{Jkq} for neighboring values of k will overlap. That is, an overall grid (regularly or irregularly spaced) will be specified with a total number of samples on the order of the number of scaling functions to be included on the finest level. From this set are chosen r quadrature points in the neighborhood of each $\phi_{Jk\alpha}$. In the common case that the samples are uniformly spaced as in Eq. (39), the Lagrange derivatives and quadrature coefficients are the same for all values of k and need to be calculated only once. As an example, taking sample points for $\phi_{Jk\alpha}$ symmetrically distributed at $x = (k+1/2)/2^J, (k+3/2)/2^J, (k+5/2)/2^J$, one calculates the weights $\omega_{J,k,1,1} = \omega_{J,k,1,3} = (7-2\sqrt{10})/24 \cdot 2^J$, $\omega_{J,k,1,2} = 1-(7-2\sqrt{10})/12 \cdot 2^J$, $\omega_{J,k,2,1} = -\omega_{J,k,2,3} = (\sqrt{6}-\sqrt{15})/12 \cdot 2^J$, $\omega_{J,k,2,2} = 0$.

Accuracy on scale j is gained by calculating the scaling function projections at finer initial levels J and using the two-scale relations iteratively to obtain the coarser scale expansion coefficients. For uniformly spaced samples, the error of any particular coefficient in the multiresolution analysis is usually asymptotically proportional to 2^{-Jr}, though symmetric distributions of sample points will improve this to $2^{-J(r+1)}$ for odd r [32]. In practice, calculation of the projection integrals may require different densities of sample points (i.e., different finest levels J) in different locations for the same degree of accuracy. It then becomes advantageous to use an adaptive wavelet quadrature scheme such as that discussed for single wavelet families in Johnson *et al.* [34], where the integrals for ranges of values k are treated in batches to maintain the linear character of the sampling relative to the number of included scaling functions.

The addition of the edge scaling functions only slightly complicates the picture. For each n, a set of sample points x_{Jnq} is chosen. These may, for instance, be the r points nearest the edge regardless of the value of n. Aside from notational changes, the differences are primarily that the edge moments M^L_{pn} are used in Eq. (42) instead of $m_{p\alpha}(-\delta)$, i.e.,

$$\left\langle \Phi^L_{Jn} \mid f \right\rangle \approx \sum_{q=1}^{r} \omega^L_{Jnq} f(x_{Jnq}), \tag{43}$$

$$\omega^L_{Jnq} = \sum_{p=0}^{r-1} 2^{-J/2-Jp} \frac{M^L_{pn}}{p!} L^{(p)}_{Jnq}(0). \tag{44}$$

A similar form holds in the case of a right-hand edge.

VI. BILINEAR MOMENTS AND GENERAL MATRIX ELEMENTS

For applications to quantum problems, it is necessary to have systematic means of evaluating Hamiltonian matrix elements in the multiwavelet basis. As for projection integrals linear in the basis functions, these bilinear integrals may be calculated by the combination of scaling function quadrature on fine scales and recursion to coarser scales (see Johnson *et al.* [34], for the single wavelet case). One starts by evaluation of the special monomial moments,

$$r_{p;\ell\beta;k\alpha} = \int_0^\infty dx\, \phi_\beta(x-\ell)x^p\phi_\alpha(x-k). \tag{45}$$

Setting the lower integration limit to 0 has no consequence if at least one of the scaling functions vanishes there anyway, i.e., either k or $\ell \geq 0$, but a truncation occurs if k and ℓ both have one of the values -2 or -1. Through use of the two-scale relations in Eq. (1) on both bra and ket scaling functions, one finds that these moments must satisfy

$$r_{p;\ell,\beta;k,\alpha} = 2^{-p-1}\sum_{\ell'=0}^{3}\sum_{\beta'=1}^{2}\sum_{k'=0}^{3}\sum_{\alpha'=1}^{2} c_{\ell';\beta\beta'}r_{p;2\ell+\ell',\,\beta';2k+k',\alpha'}c_{k';\alpha\alpha'}, \tag{46}$$

where $c_{k';\alpha\alpha'}$ is the (α,α') element of the matrix $\mathbf{c}_k$.

Focusing first on the regular case that either k or $\ell \geq 0$, we may use change of variables in Eq. (45) to express each moment in the form

$$\begin{aligned} r_{p;\ell\beta;k\alpha} &= \int dx\, \phi_\beta(x)(x+\ell)^p\phi_\alpha(x-k+\ell) \\ &= \sum_{p'=0}^{p}\binom{p}{p'}\ell^{p-p'}r_{p';0\beta;k-\ell,\alpha}, \end{aligned} \tag{47}$$

so it is sufficient to consider the $\ell = 0$ case and to express all moments in Eq. (46) in terms of those with first spatial index equal to zero. Thus, the number of independent quantities that must be determined is reduced to $r_{p;0\beta;k\alpha}$ for $-2 \leq k \leq 2$. There are even more constraints, however. From Eq. (45), it can be shown that there is a further relationship between the integrals for positive and negative values of k,

$$r_{p;0\beta;-k\alpha} = \sum_{p'=0}^{p}\binom{p}{p'}(-k)^{p-p'}r_{p';0\alpha;k\beta}. \tag{48}$$

Also, the symmetry/antisymmetry of the Chui–Lian multiscaling functions leads to a relation for fixed k,

$$r_{p;0,2;k1} = \sum_{p'=0}^{p}\binom{p}{p'}(k+3)^{p-p'}(-1)^{p'+1}r_{p';0,1;k2}. \tag{49}$$

Thus it is only necessary to find the moments for $k \geq 0$ and for $\alpha \geq \beta$. One may solve these equations for successive values of p, the starting values ($p = 0$) being provided by

TABLE IV
Scaling Function Matrix Elements $r_{p;0\beta;k\alpha}$

p	k	$r_{p;01;k1}$	$r_{p;01;k2}$	$r_{p;02;k2}$
0	k	$\delta_{k,0}$	0	$\delta_{k,0}$
1	0	1.5	0.2513953839897815	1.5
1	1	0	−0.7078901071877632e-2	0
1	2	0	0.56760290068037941e-5	0
2	0	2.320425914524887	0.7541861519693444	2.356088676074920
2	1	−0.7058932129758992e-2	−0.2043311742771540e-1	0.8418566994621792e-2
2	2	−0.1049681338301419e-4	0.4160018853613721e-4	0.1660847650782450e-4
3	0	3.691916615361994	1.731044277705884	3.852399042337138
3	1	−0.4235359277855395e-1	−0.3793828760959689e-1	0.5051140196773075e-1
3	2	−0.7872610037260640e-4	0.2056171598391129e-3	0.1245635738086838e-3

the orthogonality relations,

$$r_{0;0\beta;k\alpha} = \delta_{k0}\delta_{\alpha\beta}. \tag{50}$$

The first few essential matrix moments are given in Table IV.

For evaluation of the moments with truncated integrals, it is only necessary to return to Eq. (46) for the various cases of $k, \ell = -2, -1$ and replace those moments with k or $\ell \geq 0$ by the values just calculated. The resulting inhomogeneous equations for the edge moments are then readily solved. From the accumulated bilinear moments, those involving the primitive edge scaling functions $\phi_p^L(x)$ may be calculated using Eq. (15), and then those involving the orthogonal edge scaling functions $\Phi_p^L(x)$ may be calculated using Eqs. (21) and (22). The final moments come in two flavors,

$$r^{LL}_{p;n;m} = \int_0^\infty dx\, x^p \Phi_n^L(x)\Phi_m^L(x), \qquad n = 0, 1, 2, \quad m = 0, 1, 2, \tag{51}$$

$$r^{L}_{p;n;k\alpha} = \int_0^\infty dx\, x^p \Phi_n^L(x)\phi_{k\alpha}(x), \qquad n = 0, 1, 2, \quad k = 1, 2, \tag{52}$$

given in Tables V and VI, respectively.

TABLE V
Edge—Edge Scaling Function Matrix Elements $r^{LL}_{p;n;m}$

n	m	$p = 0$	$p = 1$	$p = 2$	$p = 3$
0	0	1	0.2990514754096211	0.2662123389639531	0.3503025685821318
0	1	0	−0.2543568724785701	−0.4201074139897117	−0.6393816813968993
0	2	0	0.06562045428344967	−0.2128662044878927	0.5054843507387799
1	1	1	0.9221737384641544	1.052971930015515	1.411629796564526
1	2	0	−0.2312149291328620	−0.6322048667407890	−1.363804807971201
2	2	1	1.617302572198752	2.688321806415069	4.563829763649434

TABLE VI
Mixed Scaling Function Matrix Elements $r^{L\ a}_{p;n;k\alpha}$

n	k	α	$p=1$	$p=2$	$p=3$
0	1	1	−0.002343791357064710	−0.01124904571980595	−0.03947047214560973
0	1	2	0.0007305592353298863	0.00488861923960781	0.02060204766022266
0	2	1	0.1876503312276107e-5	0.6091049653125483e-5	0.1051208572573486e-4
0	2	2	−0.5835098282189144e-6	0.1214183772481723e-5	0.2004294288982571e-4
1	1	1	0.004069194912957392	0.02045406508253334	0.07407645110083808
1	1	2	−0.0003363996019236961	−0.00579413228263492 6	−0.03075961533726273
1	2	1	−0.3261767309182364e-5	−0.9217342837047419e-5	−0.7995661625196105e-5
1	2	2	0.2733383574047245e-6	−0.7540845629055856e-5	−0.6167944804718003e-4
2	1	1	−0.002060549154200186	−0.01720020152886713	−0.07855369208918476
2	1	2	−0.006677911494492028	−0.01682116081869723	−0.02106659248260412
2	2	1	1.652638376802516e-5	−0.5489237626273993e-5	−0.7214429812333357e-4
2	2	2	5.355076395925271e-5	0.4408363541712476e-4	0.0002302585381633707

[a] Those for $p = 0$ vanish.

For more general functions $f(x)$, integrals bilinear in the regular scaling functions may be calculated by quadrature in similar fashion as was accomplished above for linear integrals,

$$\langle \phi_{J\ell\beta} | f | \phi_{Jk\alpha} \rangle \approx \sum_{q=1}^{r} \omega_{J;\ell\beta;k\alpha;q} f(x_{J\ell kq}). \tag{53}$$

It is assumed that the positions $x_{J\ell kq}$ are the same for all α and β, but depend upon both the bra and ket scaling function positions, k and ℓ, as well as the scale J. Using Lagrange interpolation of $f(x)$ as before and expanding around a prechosen point $\eta_{\ell k}/2^J$ leads to the following form for the quadrature weights

$$\omega_{J;\ell\beta;k\alpha;q} = \sum_{p=0}^{r-1} \frac{1}{p!} L_{J\ell kq}\left(\frac{\eta_{\ell k}}{2^J}\right) 2^{-Jp} \int_0^\infty dx \phi_{\ell\beta}(x)(x-\eta_{\ell k})^p \phi_{k\alpha}(x), \tag{54}$$

$$L_{J\ell kq}(x) = \prod_{q'\neq q}^{r} \frac{x - x_{J\ell kq'}}{x_{J\ell kq} - x_{J\ell kq'}}. \tag{55}$$

The weights, therefore, can be evaluated in terms of linear combinations of the moments $r_{p;0\beta;k\alpha}$ calculated above, although the specific details depend upon which choice of shift $\eta_{\ell k}$ is made. This may be, for instance, an endpoint or centerpoint of the region of common support of $\phi_{k\alpha}$ and $\phi_{\ell\beta}$. Under most choices, one may at least assume translation-invariance; that is, $\eta_{\ell k}$ is only a function of the difference $k-\ell$. The same then becomes true of $\omega_{J;\ell\beta;k\alpha;q}$, so one reduces the number of independent weights that must be calculated to a small number, no matter how many values of k and ℓ are included. For those integrals involving the edge functions, the weights are defined similarly, but in terms of $r^{LL}_{p;n;m}$ and $r^{L}_{p;n;k\alpha}$.

For the all-important issue of systematic accuracy, adaptive refinement is again required. For the case of single wavelet families, a method was outlined by Johnson *et al.* [34], which maintains linear scaling with respect to the number of function samples that must be

evaluated. Aside from the multiple scaling functions for each spatial index and the inclusion of special functions near the boundaries, the discussion given there also applies to the current work.

VII. KINETIC ENERGY MATRIX ELEMENTS AND REGULARIZATIONS

It is also necessary to evaluate the basis set representation of the kinetic energy operator K. This is a second-order differential operator whose precise form depends on the coordinates employed. For a given wave function $F(x)$, expansion of the product $KF(x)$ in the regular multiwavelet basis requires insertion of a resolution of the identity operator, which takes the form

$$\mathbf{I} = \sum_{k=-\infty}^{+\infty} \sum_{\alpha=1}^{2} |\phi_{Jk\alpha}\rangle\langle\phi_{Jk\alpha}| + \sum_{j=J}^{+\infty} \sum_{k=-\infty}^{+\infty} \sum_{\alpha=1}^{2} |\psi_{jk\alpha}\rangle\langle\psi_{jk\alpha}|. \tag{56}$$

In most Wavelet-Galerkin methods, it is assumed that J is chosen to give sufficiently fine resolution that the wavelet components of $F(x)$ at that and finer scales may be neglected. The operator K is then approximated by its projection on the scaling function subspace, and it is only necessary to calculate the matrix elements $\langle\phi_{J\ell\beta}|K|\phi_{Jk\alpha}\rangle$. This procedure is briefly described.

The particular differential operators that will be considered for the quantum mechanical applications are of the form $-\frac{d}{dx}x^p\frac{d}{dx}$ with p an integer. We assume $J = 0$ without loss of generality. Using integration by parts and neglecting wavelet components in the resolution of the identity, the scaling function projections of such an operator applied to a function $F(x)$ can be written as

$$\begin{aligned}\int dx\, \phi_{\ell\beta}(x)\left(-\frac{d}{dx}x^p\frac{d}{dx}\right)F(x) &= \int dx \left[\frac{d}{dx}\phi_{\ell\beta}(x)\right]x^p\left[\frac{d}{dx}F(x)\right] \\ &\approx \sum_{k=-\infty}^{+\infty}\sum_{\alpha=1}^{2} d_{p;\ell\beta;k\alpha}\int dx\, \phi_{k\alpha}(x)F(x),\end{aligned} \tag{57}$$

where the latter integrals are the projection integrals discussed earlier and the new integrals are components of a hermitian matrix,

$$d_{p;\ell\beta;k\alpha} = \int dx\, [d\phi_{\ell\beta}(x)/dx]x^p[d\phi_{k\alpha}(x)/dx]. \tag{58}$$

This is a band matrix in the spatial indices since the only nonzero elements occur for $|k-\ell| \le 2$. The calculation of similar matrices in single scaling function bases has been addressed by Beylkin [4] (see also Resnikoff and Wells [54]), and the generalization to the multiwavelet case is not difficult. First, under a shift of integration variable, the integrals in Eq. (58) can all be expressed in terms of integrals with vanishing first spatial index,

$$\begin{aligned} d_{p;\ell\beta;k\alpha} &= \int dx[d\phi_{0\beta}(x)/dx](x+\ell)^p[d\phi_{k-\ell,\alpha}(x)/dx] \\ &= \sum_{p'=0}^{p}\binom{p}{p'}\ell^{p-p'}d_{p';0\beta;k-\ell,\alpha}, \end{aligned} \tag{59}$$

so it is again only necessary to consider the $\ell = 0$ case. Using the refinement equations, one obtains the relations

$$d_{p;0\beta;k\alpha} = 2^{1-p} \sum_{\ell'=0}^{3} \sum_{\beta'=1}^{2} c_{\ell';\beta\beta'} \sum_{k'=0}^{3} \sum_{\alpha'=1}^{2} c_{k';\alpha\alpha'} \sum_{p'=0}^{p} \binom{p}{p'} (\ell')^{p-p'} d_{p';0\beta';2k+k'-\ell',\alpha'}. \quad (60)$$

The symmetry of the full matrix under the interchange $(\ell\beta) \leftrightarrow (k\alpha)$ leads to

$$d_{p;0\alpha;-k,\beta} = \sum_{p'=0}^{p} \binom{p}{p'} (-k)^{p-p'} d_{p';0\beta;k,\alpha}, \quad (61)$$

allowing attention to be further restricted to $k \geq 0$. A final constraint arises from the symmetry and antisymmetry of the scaling functions ϕ_1 and ϕ_2, respectively, under the reflection $x \to 3 - x$,

$$d_{p;02;k1} = \sum_{p'=0}^{p} \binom{p}{p'} (k+3)^{p-p'} (-1)^{p'+1} d_{p';01;k,2}, \quad (62)$$

making it possible to restrict attention to $\alpha \geq \beta$.

Equations (60)–(62) yield a homogeneous system to which must be added inhomogeneous constraints. These may be obtained from the equations for polynomial expansion. For the case $p = 0$, we start from the relation

$$\left(x - \frac{3}{2}\right)^2 = \sum_{k} \sum_{\alpha=1}^{2} m_{2\alpha} \left(k - \frac{3}{2}\right) \phi_{k\alpha}(x). \quad (63)$$

Differentiating twice, we have

$$2 = \sum_{k} \sum_{\alpha=1}^{2} m_{2\alpha} \left(k - \frac{3}{2}\right) \phi^{(2)}_{k\alpha}(x). \quad (64)$$

Projection onto $\phi_\beta(x)$ and use of integration by parts on the right-hand side gives

$$2m_{0\beta} = -\sum_{k} \sum_{\alpha=1}^{2} m_{2\alpha} \left(k - \frac{3}{2}\right) d_{0;0\beta;k\alpha}. \quad (65)$$

Since $\hat{\mathrm{m}}_0 = [1, 0]^T$, only the $\beta = 1$ equation is inhomogeneous. For differential operators with higher p, we proceed in a slightly different manner,

$$x - \frac{3}{2} = \sum_{k} \sum_{\alpha=1}^{2} m_{1\alpha} \left(k - \frac{3}{2}\right) \phi_{k\alpha}(x), \quad (66)$$

$$\frac{d}{dx} x^p \frac{d}{dx} \left(x - \frac{3}{2}\right) = p x^{p-1} = \sum_{k} \sum_{\alpha=1}^{2} m_{1\alpha} \left(k - \frac{3}{2}\right) \frac{d}{dx} x^p \frac{d}{dx} \phi_{k\alpha}(x), \quad (67)$$

$$p m_{p-1,\beta}(0) = -\sum_{k} \sum_{\alpha=1}^{2} m_{1\alpha} \left(k - \frac{3}{2}\right) d_{p;0\beta;k\alpha}. \quad (68)$$

With these results, the banded scaling function matrices $d_{p;\ell\beta;k\alpha}$ may be evaluated either numerically or analytically. Within the scaling function subspace, this gives the exact representations of the differential operators.

A caveat we wish to stress here is that all of the differential matrix elements considered are defined with respect to the hermitian form where one derivative acts upon the bra and the other upon the ket. For all functions which vanish at the endpoints of their support, integration by parts can be employed so that both derivatives are acting upon the same function. The edge functions offer an exception to this, however, since $\Phi_0^L(0) = 2.183415683967980 \neq 0$. In extension of the above methods to the integrals over the edge scaling functions, integration by parts in the $p = 0$ case can lead to the appearance of surface terms which must not be neglected. In such a case, the form of the operator with derivatives split between bra and ket is the one that is to be calculated because, as pointed out in a similar situation by Slater [57], this is the form that enters the variational principle from which Schrödinger's equation is derived. This is, in any case, seen to be the natural choice to avoid non-Hermiticity of the kinetic energy operator.

For functions $F(x)$ containing components outside the scaling function subspace, e.g., polynomials of higher than second order, the neglected wavelet components can become more significant. Thus, application of the matrix $\mathbf{d}_p$ to the array of coefficients for the function x^3 will not quite produce the projections for $-(d/dx)x^p(d/dx)x^3 = -3(p+2)x^{p+1}$. In practice, it is found that convergence of kinetic energy matrix elements with respect to scale refinement is quite slow compared to that for potential matrix elements using the Chui–Lian family. We attribute this fact to the derivative discontinuities which occur for scaling functions and wavelets with such short support [18] . A different approximate operator may, in fact, be more appropriate (see Lazaar *et al.* [40]). (This is similar in spirit to the use of higher-order operators to represent the kinetic energy in finite difference schemes.) We have found that a somewhat better alternative is to consider a matrix similar to $\mathbf{d}_p$, but which is regularized by requiring it to take projections of x^i into those of $-i(i+p-2)x^{i+p-2}$ for powers i exceeding 2. Such a matrix implicitly includes selective contributions from the neglected wavelets. Operationally, we may simply ask for a matrix $\tilde{\mathbf{d}}_p$ that has the same form and symmetries as $\mathbf{d}_p$ as well as obeying

$$\int dx \left[\frac{d}{dx}\phi_{\ell\beta}(x)\right] x^p \frac{d}{dx} x^i = -i(i+p-1)\int dx\, \phi_{\ell\beta}(x) x^{i+p-2}$$
$$= \sum_{k=\ell-2}^{\ell+2}\sum_{\alpha=1}^{2} \tilde{d}_{p;\ell\beta;k\alpha}\int dx\, \phi_{k\alpha}(x) x^i. \tag{69}$$

It again follows that it is sufficient to consider only $\ell = 0$. One finds using Eq. (8),

$$-i(i+p-1)m_{i+p-2,\beta}(0) = \sum_{k=-2}^{2}\sum_{\alpha=1}^{2} \tilde{d}_{p;0\beta;k\alpha} m_{i\alpha}(k). \tag{70}$$

These inhomogeneous equations for the elements $\tilde{d}_{p;0\beta;k\alpha}$ take the place of using refinement equations plus auxiliary inhomogeneous conditions. The power of x is allowed to vary from $i = 0$ up to the maximum power for which the equations can be solved in each case: $i \leq 7$ for $p = 0$ and $i \leq 5$ for $p = 1$ and 2. For $p = 2$, two of the nine independent parameters are undetermined, so the specific conditions $\tilde{d}_{2;02;k1} = 0$ are imposed for $k = 1$ and 2. Only these regularized results, given in Table VII, are used in the calculations below.

TABLE VII
Independent Elements of Regularized Matrices $\tilde{d}_{p;0\beta;k\alpha}$

k	β	α	$p=0$	$p=1$	$p=2$
0	1	1	4.977182345309676	7.465773517964514	3.226139691715332
0	1	2	0.0	2.942600803528535	8.827802410585606
0	2	2	18.63066834704280	27.94600252056420	−18.00780183338870
1	1	1	−2.463456034556223	−4.926912069112446	−5.707349338588092
1	1	2	3.199227390239490	6.576959085211076	1.428034437856777
1	2	2	4.491551106944728	8.983102213889456	−4.566217341489810
2	1	1	−0.02513513809861494	−0.06283784524653735	0.3236900266002465
2	1	2	0.04844069359172701	0.1193514161944246	−0.01750317784892953
2	2	2	0.08615408196204041	0.2153852049051010	0.3267301350603069

For those $\phi_{\ell\beta}$ ($\ell = 1$ and 2) sharing support with the edge functions ϕ_n^L, extra terms appear,

$$\int \left[\frac{d}{dx}\phi_{\ell\beta}(x)\right] x^p \frac{d}{dx} x^i \, dx$$
$$= \sum_{n=0}^{2} \tilde{d}^L_{p;n;\ell\beta} \int dx \phi_n^L(x) x^i + \sum_{k=1}^{\ell+2} \sum_{\alpha=1}^{2} \tilde{d}_{p;\ell\beta;k\alpha} \int dx \phi_{k\alpha}(x) x^i. \tag{71}$$

In terms of the moments of both [Eqs. (8) and (27)],

$$-i(i+p-1)m_{i+p-2,\beta}(\ell) = \sum_{n=0}^{2} \tilde{d}^L_{p;n;\ell\beta} M^L_{in} + \sum_{k=1}^{\ell+2} \sum_{\alpha=1}^{2} \tilde{d}_{p;\ell\beta;k\alpha} m_{i\alpha}(k). \tag{72}$$

Similarly,

$$\int \left[\frac{d}{dx}\Phi_n^L(x)\right] x^p \frac{d}{dx} x^i dx$$
$$= \sum_{m=0}^{2} \tilde{d}^{LL}_{p;n;m} \int dx \, \Phi^L_m(x) x^i + \sum_{k=1}^{2} \sum_{\alpha=1}^{2} \tilde{d}^L_{p;n;k\alpha} \int dx \, \phi_{k\alpha}(x) x^i, \tag{73}$$

$$-i(i+p-1)M_{i+p-2,n} - \delta_{n0}\delta_{p0}\delta_{i1}\Phi_n^L(0)$$
$$= \sum_{m=0}^{2} \tilde{d}^{LL}_{p;n;m} M^L_{im} + \sum_{k=1}^{2} \sum_{\alpha=1}^{2} \tilde{d}^L_{p;n;k\alpha} m_{i\alpha}(k). \tag{74}$$

As mentioned for the nonregularized matrix elements, integration by parts has led to a surface term in one case that must not be neglected. The solutions to these equations are given in Tables VIII and IX.

VIII. PARTICLE IN A BOX

For quantum applications with hard potential walls, all of the elements are now in place for construction of the Hamiltonian matrix in a multiscaling function basis with automatic

TABLE VIII
Independent Elements of Regularized Matrices $d^{LL}_{p;n;m}$ [a]

n	m	$p=0$	$p=1$	$p=2$
0	0	9.435321907592814	4.466395237669606	0.1208309996876746
0	1	−5.914549953627489	−4.548532761501762	0.1996808707142588
0	2	1.160556431179330	2.968767888148979	−0.8042897709301313
1	1	6.502312157886537	7.796557414440308	1.656426462479337
1	2	−3.968423454492193	−7.065469376551835	−1.445969667202100
2	2	5.580657274342218	10.19346842076509	6.118635700564971

[a] The others are obtained by symmetry.

solution of the boundary value conditions. The prototypical example is the square well potential with infinitely high walls,

$$H = -\frac{\hbar^2}{2m}\frac{d^2}{dx^2} + V(x), \tag{75}$$

$$V(x) = \begin{cases} 0 & 0 \le x \le a \\ \infty & \text{otherwise.} \end{cases} \tag{76}$$

The boundary conditions on the eigenfunctions are $\chi(0) = \chi(a) = 0$. The solutions are simple sine functions with eigenvalues $E_i = i^2\hbar^2\pi^2/2ma^2$, $i = 1, 2, 3, \ldots$. The interval from 0 to a is partitioned to include both left- and right-hand edge functions and N pairs of inner functions, $k = 1, 2, \ldots, N$ and $\alpha = 1, 2$. Including the endpoints, the total number of grid points is then $N + 5$, the spacing is $\lambda = a/(N + 4)$, and the functions used are the scaled functions $\lambda^{-1/2}\phi_{k\alpha}(x/\lambda)$, and so forth. Since the edge functions were constructed such that only Φ_0^L is nonzero at the left-hand boundary and its mirror image Φ_0^R is nonzero at the right-hand boundary, the boundary conditions are automatically satisfied by simply

TABLE IX
Elements of Regularized Matrices $d^{L}_{p:n:k\alpha}$

n	k	α	$p=0$	$p=1$	$p=2$
0	1	1	−0.7871145892092598	−1.522789767466662	0.6767795864632790
0	1	2	1.127110132528552	2.249453980557797	−1.748999704782829
0	2	1	−0.0134306082242123	−0.03415517812499165	−0.0332761357618862
0	2	2	0.0235028396104836	0.05893703602596143	0.1098168202124811
1	1	1	1.689178406657409	3.290713670616233	0.1049313899444405
1	1	2	−2.369568352156211	−4.760660569793535	2.524228398688135
1	2	1	0.02662633916236833	0.06757167950484340	0.01558781677703667
1	2	2	−0.04717626850699945	−0.1180249606514474	−0.1886005096280935
2	1	1	−3.263500213100282	−6.471271469490617	−5.312326283193022
2	1	2	4.340521773746394	8.842019478577988	−0.009986675787782307
2	2	1	−0.03781790644683623	−0.09505439042299998	0.3053868856141527
2	2	2	0.07078631144103524	0.1753144330150280	0.07861762245597229

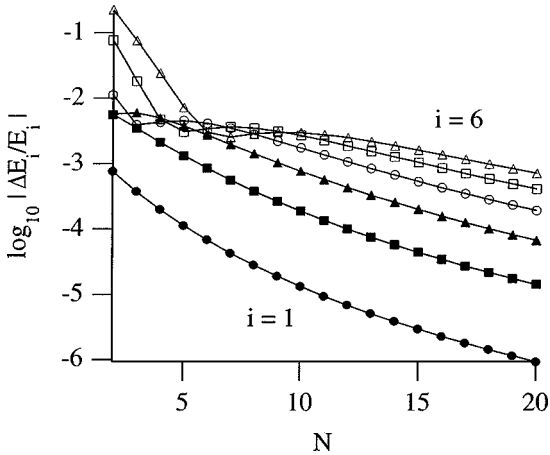

FIG. 4. Relative error for particle in a box eigenvalues as a function of the number N of pairs of multiscaling functions.

deleting these functions from the basis. There are thus $2N$ internal scaling functions and 4 edge functions included.

The fractional error in the eigenvalues is plotted in Fig. 4. It is seen that systematic decrease in error is obtained for all eigenvalues except at the lowest values of N. These deviations from monotonic decrease are possible since the basis changes in going from N to $N+1$; i.e., the spacing changes from $a/(N+4)$ to $a/(N+5)$. If one examines the error as the spacing is decreased by a factor of 2 (i.e., $N \to 2N+4$) each time, then the consecutive bases are commensurate and the smaller basis is exactly contained within the larger basis through the recursion relations in Eqs. (23)–(25). The eigenvalue error then decreases monotonically and is asymptotically proportional to λ^5.

One can use the methods developed above to handle numerically a wide variety of potential shapes on the interval, with or without the infinite walls. With transition to a multiresolution basis including wavelets at different scales, one can efficiently accommodate strongly nonpolynomial behavior. For multidimensional problems in Cartesian coordinates, the generalization is immediate since the basis functions are just products of those for the individual degrees of freedom.

IX. CURVILINEAR COORDINATES AND THE HYDROGEN ATOM

The hydrogen atom has so far provided a difficult testing ground for wavelet technology. Three dimensional calculations [60] have very slow convergence because of the singular nature of the potential, and even one-dimensional calculations [20, 22] with the potential $-1/|x|$ have only been carried to about three significant digits of accuracy. The natural approach is to separate variables in, for example, spherical polar coordinates. (For s-waves, this is equivalent to the particular one-dimensional method of [22].) In atomic units and using the variables ϕ, $z = \cos\theta$, and r, we have the eigenvalue equations

$$-\frac{d^2}{d\phi^2}F_m(\phi) = m^2 F_m(\phi), \quad 0 \le \phi \le 2\pi, \tag{77}$$

$$\left[-\frac{1}{2}\frac{d}{dz}(1-z^2)\frac{d}{dz} + \frac{1}{2}\frac{m^2}{1-z^2} \right] Q_{\ell m}(z) = \ell(\ell+1) Q_{\ell m}(z), \quad -1 \le z \le 1, \quad (78)$$

$$\left[-\frac{1}{2}\frac{d^2}{dr^2} + \frac{\ell(\ell+1)}{2r^2} - \frac{1}{r} \right] R_{n_r \ell}(r) = -\frac{1}{2n_r^2} R_{n_r \ell}(r), \quad 0 \le r < \infty, \quad (79)$$

with volume elements $d\phi$, dz, and dr, respectively. We examine each of these individually.

A. *Azimuthal Angle*

The first of these equations has the boundary conditions of continuity of F_m and its derivative at the boundaries, i.e., $F_m(0) = F_m(2\pi)$, $F'_m(0) = F'_m(2\pi)$. In this situation, one need go no further than to use the existing method of periodizing the multiscaling functions, i.e., allowing them to wrap at the domain edges. The edge functions constructed in this paper are not needed.

B. *Polar Angle*

In the second equation, we consider the $m = 0$ case for which the solutions are normalized multiples of the Legendre polynomials, $P_0 = 1$, $P_1 = z$, $P_2 = 3z^2/2 - 1/2$, and so forth. The boundary conditions are now regularity of the solution at the interval endpoints $z = \pm 1$, automatically satisfied by the three left-hand edge functions at $z = -1$ and the three right-hand edge functions at $z = +1$. All of the derivative matrix elements can be expressed in terms of the integrals calculated above. Diagonalization of the banded matrix for different numbers N of pairs of inner multiscaling functions yields eigenvalues which are exact for the first three eigenvalues, i.e., those for which the eigenfunctions are completely in the multiscaling function subspace. The errors of higher eigenvalues, shown in Fig. 5, decrease systematically with increasing N (monotonically in this case). For sequences which halve the spacings in each step, the error is found to be asymptotically proportional to λ^6.

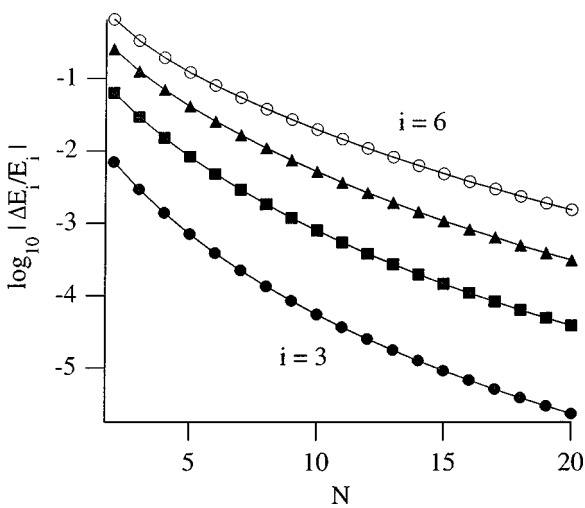

FIG. 5. Relative error for Legendre eigenvalues as a function of the number N of pairs of multiscaling functions.

C. *Radius*

The radial equation differs by virtue of possessing only one explicit domain edge, that at $r = 0$. One may *choose* for convenience to impose a right-hand edge at some value of r, though this is not important for the present demonstration. The first-order singularity $-1/r$ requires that we again exclude the Φ_0^L basis function. (For the case of volume element dr, the eigenfunctions have leading order $r^{\ell+1}$.) Thus, only the two left-hand functions Φ_1^L and Φ_2^L are added to the regular multiscaling functions.

New bilinear integrals are required. The starting point is the generalization of the integrals $r_{p;\ell\beta;k\alpha}$ [Eq. (45)] between regular multiscaling functions to negative powers p. These functions do not overlap the origin, so their integrals may be evaluated using regular quadrature on scale J as in Eq. (53) with $f(r) = 1/r$, followed by recursion to scale $j = 0$. Those integrals involving the lowest k and ℓ will still be more difficult to converge, however, and are best calculated separately to higher order. (This is an example where adaptive wavelet quadrature [34] would be of use, though it is not presently coded.) Those integrals involving the edge functions can once more be calculated by using the edge recursions, substituting the values determined for integrals involving only regular multiscaling functions, and solving the resulting inhomogeneous equations for those involving edge functions.

Table X shows the exact and calculated hydrogenic energies as functions of n_r. The spacing λ may be varied for optimization of the eigenvalues, important since only a single scale is used in the present calculations, and the eigenfunctions all have dramatically different outward reaches (i.e., the expectation value $\langle r \rangle$ increases as n_r^2 so that excited states quickly become diffuse). Different scale optimization criteria are accordingly considered. The third column shows the results for an especially small scale with λ chosen to minimize the 1s eigenvalue. The multiscaling function basis is thus shown to be able to reproduce individual eigenvalues to several significant figures, and more can be obtained systematically by increasing the density of basis functions. Excited states will each require different optimal values of λ for a fixed number of basis functions. The fourth column has a significantly larger λ chosen according to a more democratic simultaneous optimization of the first several eigenvalues, balancing the density and range of basis functions to achieve errors of similar magnitude for each state.

The extension to p, d, f, . . . , waves is also allowed by the same machinery. The presence of the centrifugal barrier term $\sim 1/r^2$ additionally requires discarding of Φ_1^L, the function which is linear in r as $r \to 0$. The matrix elements of $1/r^2$ are calculated using the same

TABLE X

Eigenvalues of s-Wave and p-Wave Hydrogenic States for Different Values of the Important Scale Parameter λ

		s wave ($\ell = 0$)		p wave ($\ell = 1$)	
n_r	E_{n_r}	$\lambda = 0.04$	$\lambda = 0.25$	$\lambda = 0.10$	$\lambda = 0.38$
1	−0.50000000	−0.49999996	−0.49981972		
2	−0.12500000	−0.12160942	−0.12498493	−0.12499987	−0.12493531
3	−0.05555556	0.01760954	−0.05555144	−0.05547890	−0.05553166
4	−0.03125000	0.22556305	−0.03124831	−0.02615612	−0.03123918
5	−0.02000000	0.50927990	−0.01998286	0.00837816	−0.01999428
6	−0.01388889	0.86504697	−0.01310821	0.05579317	−0.01388452

methods as before within the truncated basis. Using two different values of the scale parameter, again optimized according to different purposes, the results for the p wave are shown in the last columns of Table X. These results are similar to those for the s wave, a situation found for higher waves as well.

The current approach is not meant to apply directly to the solution of polyatomic electronic structure problems [1, 6, 9, 26, 28, 29, 60, 66], for which uniform multidimensional grids independent of the atomic positions have been used. (Nonuniform bases on irregular grids are also possible [26].) To use orthogonal compact support wavelets for such problems, special multidimensional quadratures have been investigated [48].

Although only the case $m = 0$ was explicitly addressed above, the associated Legendre equation in Eq. (78) for $m > 0$ can be treated in the same manner as the radial equation for $\ell > 0$ since the algebraic singularities are of the same type. The essential difference is the existence of two boundaries rather than one.

X. DISCUSSION

It has been shown that orthogonal multiwavelet families may be used for quantum problems with general potentials in a manner very similar to that taken for single wavelet families. Numerical quadrature methods are able to construct accurately and efficiently the banded potential matrices in the multiscaling function basis, the first step required before expanding in a multiresolution representation. This allows the use of bases with more localized support and greater smoothness, whose members possess definite symmetry or antisymmetry (do not have a left or right bias). It has been shown that all of the required integrals can be obtained by generalization of methods used for single wavelet families. The exception we have made is to use a regularized form for the kinetic energy operators in the multiscaling function basis rather than the simple projection (this could also be done for single scaling function bases). The applications were made to the Chui–Lian [10] multiwavelets on the interval [0,3] to be specific, but can be adapted to other multiwavelet families.

Edge scaling functions and wavelets have been derived in extension of the methods used by Cohen *et al.* [12, 13], and Monasse and Perrier [50, 51] for single wavelets. This allows the approximation order of three (quadratic polynomials) to be obtained throughout a finite interval or along a half-line. By judicious choice of the edge functions, one is able to satisfy the boundary conditions of many typical equations of quantum mechanics. The same set of basis functions was then shown to be usable for either Cartesian and curvilinear degrees of freedom.

Since this first demonstration has focused on standard problems with analytical solutions for calibration, there may be the appearance of cracking a peanut with a sledgehammer. The actual situation, however, is that the present numerical methods may be applied to a large variety of coordinates and potential functions. The next important step for increasing adaptability is implementation of the multiresolution decomposition, i.e., to transform to the multiscale wavelet basis. As discussed by Beylkin *et al.* [5] for single wavelet bases, this changes the structure of the matrices so that the sparseness is partially destroyed. Their solution to this problem is a redundant "nonstandard representation" for matrix operators which streamlines matrix–vector multiplies. The nonstandard representation has already been used in numerical calculations by, e.g., Fischer [20] and Goedecker [26], and generalizations have been discussed by Lippert *et al.* [42]. Its adaptation to the current multiwavelet basis will be explored in future work.

APPENDIX

The 2×2 coefficient matrices for the Chui–Lian multiwavelet family used here are

$$\mathbf{c}_0 = \frac{1}{40}\begin{pmatrix} 10-3\sqrt{10} & 5\sqrt{6}-2\sqrt{15} \\ 5\sqrt{6}-3\sqrt{15} & 5-3\sqrt{10} \end{pmatrix}, \quad \mathbf{c}_1 = \frac{1}{40}\begin{pmatrix} 30-\sqrt{10} & 5\sqrt{6}-2\sqrt{15} \\ -5\sqrt{6}-7\sqrt{15} & 15-3\sqrt{10} \end{pmatrix},$$

$$\mathbf{c}_2 = \frac{1}{40}\begin{pmatrix} 30+3\sqrt{10} & -5\sqrt{6}+2\sqrt{15} \\ 5\sqrt{6}+7\sqrt{15} & 15-3\sqrt{10} \end{pmatrix}, \quad \mathbf{c}_3 = \frac{1}{40}\begin{pmatrix} 10-3\sqrt{10} & -5\sqrt{6}+2\sqrt{15} \\ -5\sqrt{6}+3\sqrt{15} & 5-3\sqrt{10} \end{pmatrix}, \tag{A1}$$

$$\mathbf{d}_0 = \frac{1}{40}\begin{pmatrix} 5\sqrt{6}-2\sqrt{15} & -10+3\sqrt{10} \\ -5+3\sqrt{10} & 5\sqrt{6}-3\sqrt{15} \end{pmatrix}, \quad \mathbf{d}_1 = \frac{1}{40}\begin{pmatrix} -5\sqrt{6}+2\sqrt{15} & 30+3\sqrt{10} \\ 15-3\sqrt{10} & 5\sqrt{6}+7\sqrt{15} \end{pmatrix},$$

$$\mathbf{d}_2 = \frac{1}{40}\begin{pmatrix} -5\sqrt{6}+2\sqrt{15} & -30-3\sqrt{10} \\ -15+3\sqrt{10} & 5\sqrt{6}+7\sqrt{15} \end{pmatrix}, \quad \mathbf{d}_3 = \frac{1}{40}\begin{pmatrix} 5\sqrt{6}-2\sqrt{15} & 10-3\sqrt{10} \\ 5-3\sqrt{10} & 5\sqrt{6}-3\sqrt{15} \end{pmatrix}. \tag{A2}$$

ACKNOWLEDGMENTS

This work was performed under grants from the National Science Foundation and the Robert A. Welch Foundation.

REFERENCES

1. T. A. Arias, Multiresolution analysis of electronic structure: Semicardinal and wavelet bases, *Rev. Mod. Phys.* **71**, 267 (1999).
2. P. Auscher, Ondelettes à support compact et conditions aux limites, *J. Funct. Anal.* **111**, 29 (1993).
3. S. Bertoluzza, in *Multiscale Wavelet Methods for Partial Differential Equations*, edited by W. Dahmen, A. J. Kurdila, and P. Oswald (Academic Press, San Diego, 1997), p. 109.
4. G. Beylkin, On the representation of operators in bases of compactly supported wavelets, *SIAM J. Numer. Anal.* **6**, 1716 (1992).
5. G. Beylkin, R. Coifman, and V. Rokhlin, Fast wavelet transforms and numerical algorithms I, *Comm. Pure Appl. Math.* **44**, 141 (1991).
6. M. E. Brewster, G. I. Fann, and Z. Y. Yang, Wavelets for electronic structure calculations, *J. Math. Chem.* **22**, 117 (1997).
7. C. Canuto, A. Tabacco, and K. Urban, The wavelet element method, *Appl. Comp. Harm. Anal.* **6**, 1 (1999).
8. M.-Q. Chen, C. Hwang, and Y.-P. Shih, The computation of a Wavelet-Galerkin approximation on a bounded interval, *Int. J. Numer. Meth. Eng.* **39**, 2921 (1996).
9. K. Cho, T. A. Arias, J. D. Joannopolous, and P. K. Lam, Wavelets in electronic structure calculations, *Phys. Rev. Lett.* **71**, 1808 (1993).
10. C. K. Chui and J.-L. Lian, A study of orthonormal multi-wavelets, *Appl. Numer. Math.* **20**, 273 (1996).
11. A. Cohen, W. Dahmen, and R. DeVore, Multiscale decompositions on bounded domains, *Trans. Amer. Math. Soc.* **352**, 3651 (2000).
12. A. Cohen, I. Daubechies, B. Jawerth, and P. Vial, Multiresolution analysis, wavelets and fast algorithms on an interval, *C.R. Acad. Sci. Ser. I* **316**, 417 (1992).
13. A. Cohen, I. Daubechies, and P. Vial, Wavelets on the interval and fast wavelet transforms, *Appl. Comp. Harmonic Anal.* **1**, 54 (1993).
14. W. Dahmen, B. Han, R.-Q. Jia, and A. Kunoth, Biorthogonal multiwavelets on the interval: Cubic hermite splines, *Constructive Approximation* **16**, 221 (2000).

15. W. Dahmen, A. Kunoth, and K. Urban, A Wavelet Galerkin method for the Stokes equations, *Computing* **56**, 259 (1995).
16. W. Dahmen and C. A. Micchelli, Using the refinement equation for evaluating integrals of wavelets, *SIAM J. Numer. Anal.* **30**, 507 (1993).
17. I. Daubechies, Orthonormal bases of compactly supported wavelets, *Comm. Pure Appl. Math.* **41**, 909 (1988).
18. I. Daubechies, *Ten Lectures on Wavelets* (Soc. for Industr. & Appl. Math., Philadelphia, 1992).
19. A. R. Diaz, A Wavelet-Galerkin scheme for analysis of large-scale problems on simple domains, *Int. J. Numer. Meth. Eng.* **44**, 1599 (1999).
20. P. Fischer, Numerical solutions of Eigenvalue problems by means of a wavelet-based Lanczos decomposition, *Int. J. Quant. Chem.* **77**, 552 (2000).
21. P. Fischer and M. Defranceschi, Looking at atomic orbitals through Fourier and wavelet transforms, *Int. J. Quant. Chem.* **45**, 619 (1993).
22. P. Fischer and M. Defranceschi, Numerical solution of the Schrödinger equation in a wavelet basis for hydrogen-like atoms, *SIAM J. Numer. Anal.* **35**, 1 (1998).
23. L. Gagnon and J. M. Lina, Symmetric Daubechies' wavelets and numerical solution of NLS equations, *J. Phys. A* **27**, 8207 (1994).
24. R. Glowinksi, T. W. Pan, R. O. Wells, Jr., and X. Zhou, Wavelet and finite element solutions for the Neumann problem using fictitious domains, *J. Comput. Phys.* **126**, 40 (1996).
25. R. Glowinski, W. M. Lawton, M. Ravachol, and E. Tenenbaum, *Wavelet Solutions of Linear and Nonlinear Elliptic, Parabolic and Hyperbolic Problems in One Space Dimension*, AD890527 (Aware, Inc., 1989).
26. S. Goedecker, Wavelets and Their Application for the Solution of Partial Differential Equations in Physics (Presses Polytechniques et Universitaires Romandes, 1998).
27. S. Goedecker and O. V. Ivanoc, Frequency localization properties of the density matrix and its resulting hypersparsity in a wavelet representation, *Phys. Rev. B* **59**, 7270 (1999).
28. S. Goedecker and O. V. Ivanov, Linear scaling solution of the Coulomb problem using wavelets, *Solid State Commun.* **105**, 665 (1998).
29. S. Han, K. Cho, and J. Ihm, Wavelets in all-electron density-functional calculations, *Phys. Rev. B* **60**, 1437 (1999).
30. D. P. Hardin and D. W. Roach, Multiwavelet prefilters I: Orthogonal prefilters preserving approximation order $p \leq 2$, *IEEE Trans. Circuits Syst. II* **45**, 1106 (1998).
31. D. K. Hoffman, G. W. Wei, D. S. Zhang, and D. J. Kouri, Shannon–Gabor wavelet distributed approximating functional, *Chem. Phys. Lett.* **287**, 119 (1998).
32. B. R. Johnson, Multiwavelet moments and projection prefilters, *IEEE Trans. Signal Proc.* **48**, 3100 (2000).
33. B. R. Johnson and J. L. Kinsey, Quadrature prefilters for the discrete wavelet transform, *IEEE Trans. Signal Proc.* **48**, 873 (2000).
34. B. R. Johnson, J. P. Modisette, P. J. Nordlander, and J. L. Kinsey, Quadrature integration for orthogonal wavelet systems, *J. Chem. Phys.* **110**, 8309 (1999).
35. B. R. Johnson and W. P. Reinhardt, Adiabatic separations of stretching and bending vibrations: Application to H_2O, *J. Chem. Phys.* **85**, 4538 (1986).
36. J. Ko, A. J. Kurdila, R. O. Wells, and X. Zhou, On the conditioning of numerical boundary measures in Wavelet Galerkin methods, *Comm. Numer. Meth. Eng.* **12**, 281 (1996).
37. C. Lage and C. Schwab, Wavelet Galerkin algorithms for boundary integral equations, *SIAM J. Sci. Comput.* **20**, 2195 (1999).
38. A. Latto, H. L. Resnikoff, and E. Tenenbaum, *Compactly Supported Wavelets*, AD91078, (Aware, Inc., 1991).
39. A. Latto and E. Tenenbaum, Compactly supported wavelets and the numerical solution of Burgers' equation, *C. R. Acad. Sci. Paris* **311**, 903 (1990).
40. S. Lazaar, J. Liandrat, and P. Tchamitchian, Wavelets algorithm for the numerical resolution of variable coefficient partial differential equations, *C. R. Acad. Sci. Paris Ser. I* **319**, 1101 (1994).
41. J. Liandrat and P. Tchamitchian, Resolution of the 1D Burgers Equation Using Spatial Wavelet Approximation, 90-83 (NASA-ICASE, 1990).

42. R. A. Lippert, T. A. Arias, and A. Edelman, Multiscale computation with interpolating wavelets, *J. Comput. Phys.* **140**, 278 (1998).
43. Y. Maday, V. Perrier, and J.-C. Ravel, *C.R. Acad. Sci. Ser. I* **312**, 405 (1991).
44. S. Mallat, *A Wavelet Tour of Signal Processing* (Academic Press, San Diego, 1998).
45. S. G. Mallat, A theory for multiresolution signal decomposition: The wavelet representation, *IEEE Trans. Pattern Anal. Machine Intell.* **11**, 674 (1989).
46. Y. Meyer, Ondelettes due l'intervalle, *Rev. Mat. Iberoamericana* **7**, 115 (1992).
47. J. T. Miller and C.-C. Li, Adaptive multiwavelet initialization, *IEEE Trans. Signal Process.* **46**, 3282 (1998).
48. J. P. Modisette, (1998, unpublished).
49. J. P. Modisette, P. Nordlander, J. L. Kinsey, and B. R. Johnson, Wavelet bases in eigenvalue problems in quantum mechanics, *Chem. Phys. Lett.* **250**, 485 (1996).
50. P. Monasse and V. Perrier, Construction d'ondelettes sur l'intervalle pour la prise en compte de conditions aux limites, *C.R. Acad. Sci. Paris Ser. I* **321**, 1163 (1995).
51. P. Monasse and V. Perrier, Orthonormal wavelet bases adapted for partial differential equations with boundary conditions, *SIAM J. Math. Anal.* **29**, 1040 (1998).
52. P. M. Morse and H. Feshbach, *Methods of Theoretical Physics* (McGraw-Hill, New York, 1953).
53. Z. Qian and J. Weiss, Wavelets and the numerical solution of partial differential equations, *J. Comput. Phys.* **106**, 155 (1993).
54. H. L. Resnikoff and J. Wells, R. O., *Wavelet Analysis and the Scalable Structure of Information* (Springer-Verlag, New York, 1996).
55. J. M. Restrepo and G. K. Leaf, Wavelet-Galerkin discretization of hyperbolic equations, *J. Comput. Phys.* **122**, 118 (1995).
56. R. L. Schult and H. W. Wyld, Using wavelets to solve the Burgers equation: A comparative study, *Phys. Rev. A* **46**, 7953 (1992).
57. J. C. Slater, Wave functions in a periodic potential, *Phys. Rev.* **51**, 846 (1937).
58. F. T. Smith, *Phys. Rev.* **120**, 1058 (1960).
59. V. Strela, P. N. Heller, G. Strang, P. Topiwala, and C. Heil, The application of multiwavelet filterbanks to image processing, *IEEE Trans. Image Process.* **8**, 548 (1999).
60. C. J. Tymczak and X. Q. Wang, Orthonormal wavelet bases for quantum molecular dynamics, *Phys. Rev. Lett.* **78**, 3654 (1997).
61. O. V. Vasilyev and S. Paolucci, A dynamically adaptive multilevel wavelet collocation method for solving partial differential equations in a finite domain, *J. Comput. Phys.* **125**, 498 (1996).
62. O. V. Vasilyev and S. Paolucci, A fast adaptive wavelet collocation algorithm for multidimensional PDEs, *J. Comput. Phys.* **138**, 16 (1997).
63. T. von Petersdorff and C. Schwab, in *Multiscale Wavelet Methods for Partial Differential Equations*, edited by W. Dahmen, A. J. Kurdila, and P. Oswald (Academic Press, San Diego, 1997), p. 287.
64. M. J. Vrhel and A. Aldroubi, Projection based prefiltering for multiwavelet transforms, *IEEE Trans. Signal Process.* **46**, 3088 (1998).
65. G. W. Wei, S. C. Althorpe, D. J. Kouri, and D. K. Hoffman, An application of distributed approximating functional-wavelets to reactive scattering, *J. Chem. Phys.* **108**, 7065 (1998).
66. S. Wei and M. Y. Chou, Wavelets in self-consistent electronic structure calculations, *Phys. Rev. Lett.* **76**, 2650 (1996).
67. R. O. Wells, Jr., and X. Zhou, Wavelet solutions for the Dirichlet problem, *Numer. Math.* **70**, 379 (1995).
68. X.-G. Xia, A new prefilter design for discrete multiwavelet transforms, *IEEE Trans. Signal Process.* **46**, 1558 (1998).
69. X.-G. Xia, J. S. Geronimo, D. P. Hardin, and B. W. Suter, Design of prefilters for discrete multiwavelet transforms, *IEEE Trans. Signal Process.* **44**, 25 (1996).
70. Y. Xinxing and J. Licheng, Adaptive multiwavelet prefilter, *Electron. Lett.* **35**, 11 (1999).
71. J. C. Xu and W. C. Shann, Galerkin-wavelet methods for two-point boundary value problems, *Numer. Math.* **63**, 123 (1992).